



Contents lists available at ScienceDirect

European Journal of Medicinal Chemistry

journal homepage: <http://www.elsevier.com/locate/ejmech>

Design and synthesis of novel fluorescently labeled analogs of vemurafenib targeting MKK4

Theresa Kircher^a, Tatu Pantsar^{a,b}, Andreas Oder^c, Jens Peter von Kries^c, Michael Juchum^a, Bent Pfaffenrot^a, Philip Kloevekorn^a, Wolfgang Albrecht^d, Roland Selig^{a,d}, Stefan Laufer^{a,e,*}

^a Institute of Pharmaceutical Chemistry, Eberhard Karls University of Tuebingen, Morgenstelle 8, 72076, Tuebingen, Germany

^b School of Pharmacy, University of Eastern Finland, Yliopistoranta 1C, 70210 Kuopio, Finland

^c Leibniz-Forschungsinstitut fuer Molekulare Pharmakologie, FMP, Robert-Rössle-Straße 10, 13125, Berlin, Germany

^d HepaRegeniX GmbH, Eisenbahnstraße 63, 72072, Tuebingen, Germany

^e Tuebingen Center for Academic Drug Discovery, Morgenstelle 8, 72076, Tuebingen, Germany

ARTICLE INFO

Article history:

Received 21 July 2020

Received in revised form

18 September 2020

Accepted 29 September 2020

Available online xxx

Keywords:

Mitogen-activated protein kinase kinase 4

Vemurafenib

Fluorescence polarization assay

ABSTRACT

The mitogen-activated protein kinase kinase 4 (MKK4) plays a key role in liver regeneration and is under investigation as a target for stimulating hepatocytes to increased proliferation. Therefore, new small molecules inhibiting MKK4 may represent a promising approach for treating acute and chronic liver diseases. Fluorescently labeled compounds are useful tools for high-throughput screenings of large compound libraries. Here we utilized the azaindole-based scaffold of FDA-approved BRAF inhibitor vemurafenib **1**, which displays off-target activity on MKK4, as a starting point in our fluorescent compound design. Chemical variation of the scaffold and optimization led to a selection of fluorescent 5-TAMRA derivatives which possess high binding affinities on MKK4. Compound **45** represents a suitable tool compound for Fluorescence polarization assays to identify new small-molecule inhibitors of MKK4.

© 2020 Elsevier Masson SAS. All rights reserved.

1. Introduction

The Mitogen-Activated Protein Kinase Kinase 4 (MKK4), a member of the Mitogen-activated protein kinase family, plays an important role in the regulation of cell signaling caused by cellular stress or inflammatory cytokines. In 2013, Wüstefeld et al. demonstrated that silencing of MKK4 in mice via shRNA is substantially involved in liver regeneration and stimulates hepatocyte proliferation [1]. As a result, by this genetic silencing of MKK4, MKK7 and apoptosis signal resulting kinase 1 (ASK1) become upregulated. This leads to a higher phosphorylation of c-Jun N-terminal kinase (JNK1) and finally to enhanced activation of the transcription factors activating transcription factor (ATF2) and ETS-like transcription factor (ELK1), which are responsible for cell differentiation and increased hepatocyte proliferation [2]. At the same time, FDA-approved fibrosarcoma B (BRAF) inhibitor vemurafenib **1**

(Fig. 1) was shown to have strong off-target activity on MKK4 [3].

One method to find new lead structures for inhibiting kinases is a fluorescence polarization (FP)-based assay [4]. FP provides fast and detailed information about inhibitor-protein interaction and can be adopted for high-throughput screenings of compound libraries using competition assays [5]. The method can distinguish between bound and unbound compounds by analyzing polarized light emission after excitation [6]. Earlier, **1** has successfully been tagged with the fluorophore BODIPY to enable *in vivo* cell imaging [7].

Finding new small molecule inhibitors of MKK4 may represent a starting point for the treatment of acute and chronic liver diseases. To this end, a MKK4-targeting fluorescent could be used as a tracer for fluorescence-based competition assay systems against compound libraries. Here, we generated a series of compounds based on **1**, with varying linkers combined with a fluorophore. These efforts resulted in a MKK4-specific probe that maintains high binding affinity and meets the requirements of a tracer compound for high-throughput fluorescence polarization assays.

* Corresponding author. Auf der Morgenstelle 8, 72076, Tuebingen, Germany.

E-mail address: stefan.laufer@uni-tuebingen.de (S. Laufer).

2. Ligand design

Designing an appropriate ligand system with retaining high binding affinity is an iterative process and has strong influence on the fluorescence polarization assay results. At first, we investigated the X-ray structure of **1** bound to BRAF (PDB ID: 4rzv, 3og7) [8]. The azaindole core of **1** forms two hydrogen bonds to the hinge-region. The *para*-chloro substituent of the phenyl protrudes out of the ATP binding pocket towards the solvent in a solvent-accessible interface (Fig. 2A). On the other side of the molecule, the sulfonamide interacts with the DFG motif of BRAF forming a hydrogen bond between the NH of D592 and the sulfonamide nitrogen, whereas the terminal aliphatic propyl group occupies a lipophilic back pocket [9].

Three MKK4 structures have been published to date (PDB IDs: 3vut [10]; 3aln; 3alo [11]). Two of these structures are in complex with adenylyl-imidodiphosphate and one is an apo structure, none is in complex with inhibitors. In these structures, the lipophilic back pocket is not observed. Thus, we were first unable to observe a similar binding mode for **1** in MKK4 based on these structures. However, our molecular dynamics (MD) simulations [12], revealed the opening of this lipophilic back pocket. Docking of **1** to this MD-derived MKK4 structure resulted in a similar binding mode as observed with BRAF-**1** (Fig. 2B). This binding orientation provided us with a rational starting point for the ligand design of fluorescent derivatives for MKK4.

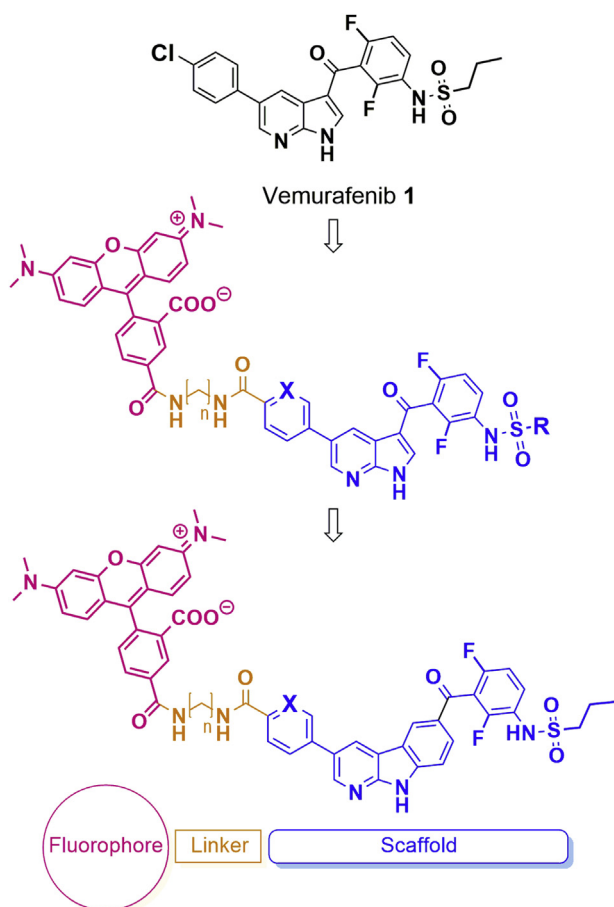


Fig. 1. Overview of the fluorophore attachment strategy. Structure of **1**; scaffold with X = CH or N and R = propyl or benzyl (highlighted in blue) attached by a linker with n = 1–6 (yellow) to the fluorophore 5-TAMRA (pink). (For interpretation of the references to color in this figure legend, the reader is referred to the Web version of this article.)

In combination with the docking results, the structural insights suggested that it might be beneficial to position the bulky fluorophore 5-TAMRA in the adjacent cleft outside the binding pocket of MKK4 (Fig. 2C). The positively charged lysine residue, K118, would be suitable for an ionic interaction with the negatively charged carboxylate group in the fluorophore (Figs. 2C and 1), fixing the ligand molecule. An optimal position for this group would be ensured by the connecting linker system with up to six carbons.

We selected the 5-Carboxytetramethylrhodamine single isomer (5-TAMRA) as a fluorophore in our synthetic strategy. Rhodamine derivatives possess high quantum yields, which can have a positive effect on the sensitivity of the fluorescent screen. As a significant number of compounds from screening libraries demonstrates a

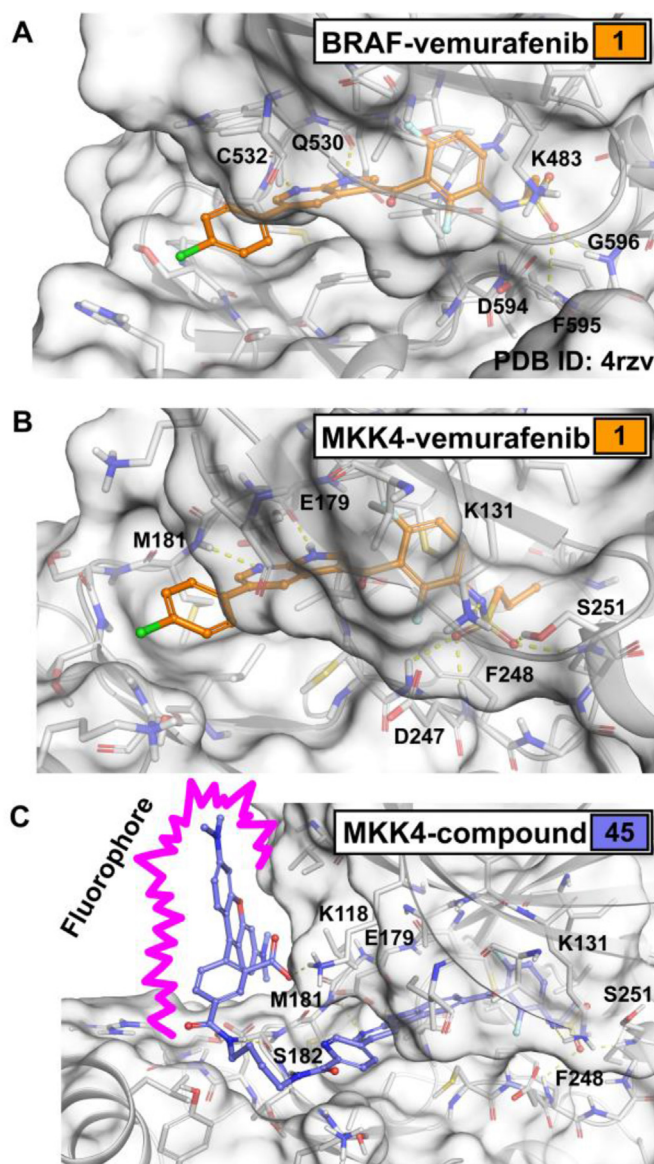


Fig. 2. Binding mode of **1** to BRAF and MKK4 as a starting point for fluorescent ligand design. (A) Crystal structure of **1** in complex with BRAF (PDB ID: 4rzv). (B) Docking pose of **1** in MD derived MKK4 structure. Similar binding mode of **1** is observed with MKK4 as with BRAF. The fluorophore occupies a cleft between the N- and C-lobe in MKK4. (C) Docking pose of fluorescent compound **45** in MKK4. In A–C: residues that show polar interactions (dashed yellow lines) with the ligand are labeled in the figures. (For interpretation of the references to color in this figure legend, the reader is referred to the Web version of this article.)

strong fluorescent emission similar to FITC (exc. 491 nm, em. 516 nm) at the used screening concentration of 10 μ M, we used 5-TAMRA (exc. 546 nm, em. 516 nm) for labelling which shows a shift to the red fluorescence like rhodamine. Thereby we prevent interference in FP-readout by most fluorescent compounds.

In order to obtain the maximum polarization effect, the local mobility should be kept as small as possible for the fluorophore bound to the target protein. Therefore, it is mandatory to minimize unfavorable repulsive interactions between the fluorophore and the protein. A screening of differing linkers is necessary to identify the best possible compromise between affinity and fluorophore mobility. Thereby the aromatic moiety of the former *para*-chloro residue serves as connection between linker and the scaffold of **1** which could be introduced via C–C-coupling. Using pyridinyl- and pyrimidinyl-moiety instead of phenyl could help to reduce the rotational movement, because this part of the molecule seems to be close to the binding cleft.

Besides the azaindole (1*H*-pyrrolo[2,3-*b*]pyridine) core of **1**, we used the α -carboline (9*H*-pyrido[2,3-*b*]indole) scaffold **B** (Fig. 3) which turned out to have a promising binding affinity to MKK4. The pyrimido[4,5-*b*]indole scaffolds were preliminarily designed by Bayer in 2003 as MKK4 and MKK7 inhibitors [13]. Due to the geometry of azaindole, we altered the structure to 9*H*-pyrido[2,3-*b*]indoles (α -carboline) to connect the linkers at the 3-position and the keto-bridge at position 6 of the three-ring system. Based on our docking results, compound **45** with this scaffold occupies the cleft nicely and forms the desired ionic interaction to K118 (Fig. 2C).

Hypothesizing that the sulfonamide part of the molecule protrudes into a lipophilic backpocket of MKK4 (see Fig. 2), the more lipophilic residue benzyl was reported to further improve binding affinity to the target and was therefore used additionally to the propyl residue [13].

3. Chemistry

The synthetic route to fluorescent azaindole derivatives **8** and **9** (Scheme 2) starts with 5-bromo-7-azaindole as commercially available starting material which was acylated with 2,6-difluoro-3-(propylsulfonamido)benzoic acid under Friedel-Crafts conditions to yield **2** described in literature [14]. For the glycine-based linkage system, the resulting bromo-derivative was directly connected to (*tert*-butoxycarbonyl)glycine under Suzuki conditions to **3** and then converted into the Boc-protected linkage mediated by HATU yielding **4**. Due to low conversion, the synthetic strategy was changed for all other linkage systems by protecting the azaindole nitrogen of **2** with 2,6-dichlorobenzoyl chloride to afford **5**. Compound **5** was then borylated with B₂pin₂ using Miyaura conditions to **6** and subsequently connected to the prepared linkage **18** (Scheme 1) to afford the corresponding Boc-protected precursor **7**.

The deprotection in TFA/toluene and amide coupling with 5-TAMRA (single isomer) afforded the fluorescent compounds **8** and **9**. The low solubility of the compounds in organic solvents and the following column chromatography resulted in low yields.

To substitute the propyl residue with benzyl, the fluorescent compounds **10** and **11** (Table 1) were prepared starting from (3-amino-2,6-difluorophenyl)(5-bromo-1*H*-pyrrolo[2,3-*b*]pyridin-3-yl)methanone (detailed reaction path can be found in SI) [14].

In Scheme 1 the synthetic route to the linkage systems is described. For the retro amide linkage with *n* = 1 commercially available 4-bromoaniline or 4-bromopyridine-2-amine were coupled using uronium salts (HATU, HBTU) or CDI to yield **12** and **13**. Retro amides have been used, as the corresponding amide with *n* = 1 is chemically not stable. For amide linkages with *n* = 2–6 containing phenyl, pyridinyl and pyrimidinyl moieties the carboxylic acid was activated with oxalyl chloride and connected to the Boc protected diamines in moderate to good yields.

Scheme 3 describes the synthesis of fluorescent α -carboline derivatives **37–47** containing scaffold B (Fig. 3) The synthesis of 3-chloro- α -carboline was prepared according to literature [15] The resulting chloro-substituted carboline was acylated (compound **23**) and further converted to the borylated species (compound **24**) in a Miyaura borylation reaction. The bromo derivatives of Boc-protected linkages were coupled in a Suzuki coupling under microwave irradiation to obtain **25–36**. After deprotection with TFA/toluene the amines were linked in a HATU-mediated amide coupling to 5-TAMRA. Low yields were isolated in some cases due to difficult column chromatography.

4. Results

The binding affinities of all compounds were characterized using a commercial binding assay (KINOMEScan by DiscoverX). The binding affinity is described by POC (percentage of control) where low numbers indicate high binding affinities (see Experimental).

Almost all of the 15 synthesized fluorescently labeled derivatives show high affinity to MKK4 (Table 1), some even higher than **1** (POC^{MKK4} = 14). Also, the scaffold change from azaindole to α -carboline is tolerated for almost all compounds (**37–47**). Only two derivatives (**9,41**) have low binding affinity to the target compared to **1**.

Changing the sulfonamide residue of **1** from propyl (**8**, POC^{MKK4} = 11) to benzyl (**10**, POC^{MKK4} = 6.6) slightly increases the affinity to the target. This confirms the hypothesis of an accessible lipophilic back pocket, just as in BRAF.

In order to identify the optimal linker length, we prepared linkage systems containing one to six carbon atoms between the fluorophore and the template. All lengths were tolerated, but for the azaindole and carboline scaffold the binding mode appeared to be different. Good binding affinity with a POC^{MKK4} of **Good binding affinity with a POC¹¹ of 11** were obtained for the azaindole scaffold, the shortest linker system (compound **33**) with one carbon and a phenylamide moiety. The carboline derivative **45** were obtained for the azaindole scaffold, the shortest linker system (compound **33**) with one carbon and a phenylamide moiety. The carboline derivative **45** (Fig. 4) was found to be the most promising, with a linker length of four carbons and a picolinamide moiety, showing a binding affinity of POC^{MKK4} = 1.3. Presumably, the additional ring system of scaffold **B** has an influence on the positioning of the former *para*-chloro residue.

Changing the phenyl moiety to pyridinyl, or pyrimidyl has nearly no impact on the binding affinity.

Comparing Boc protected compound **25** with the corresponding 5-TAMRA attached **37** (Table 2) binding affinity slightly increases. Thus, the incorporation of the bulky fluorophore 5-TAMRA has no negative effect on the binding affinity with the chosen linkers.

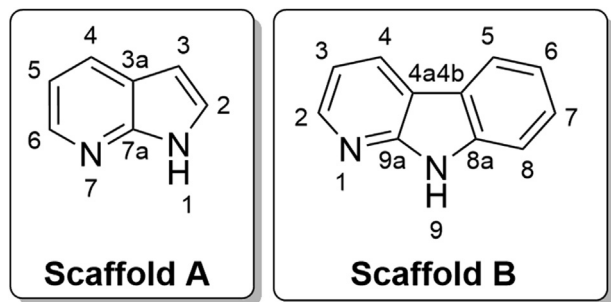
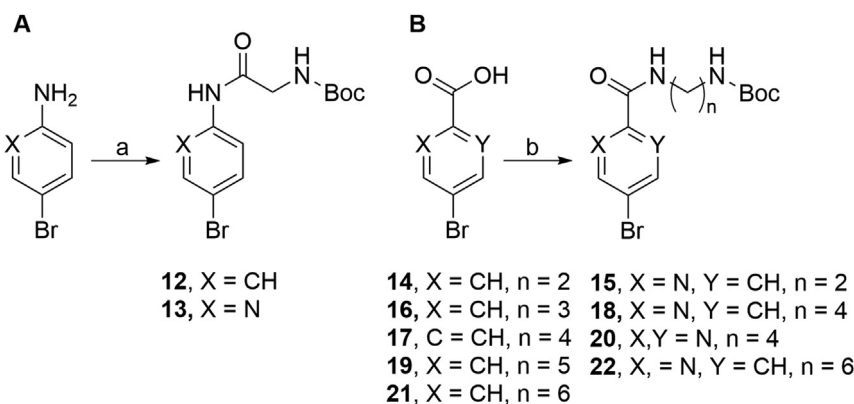
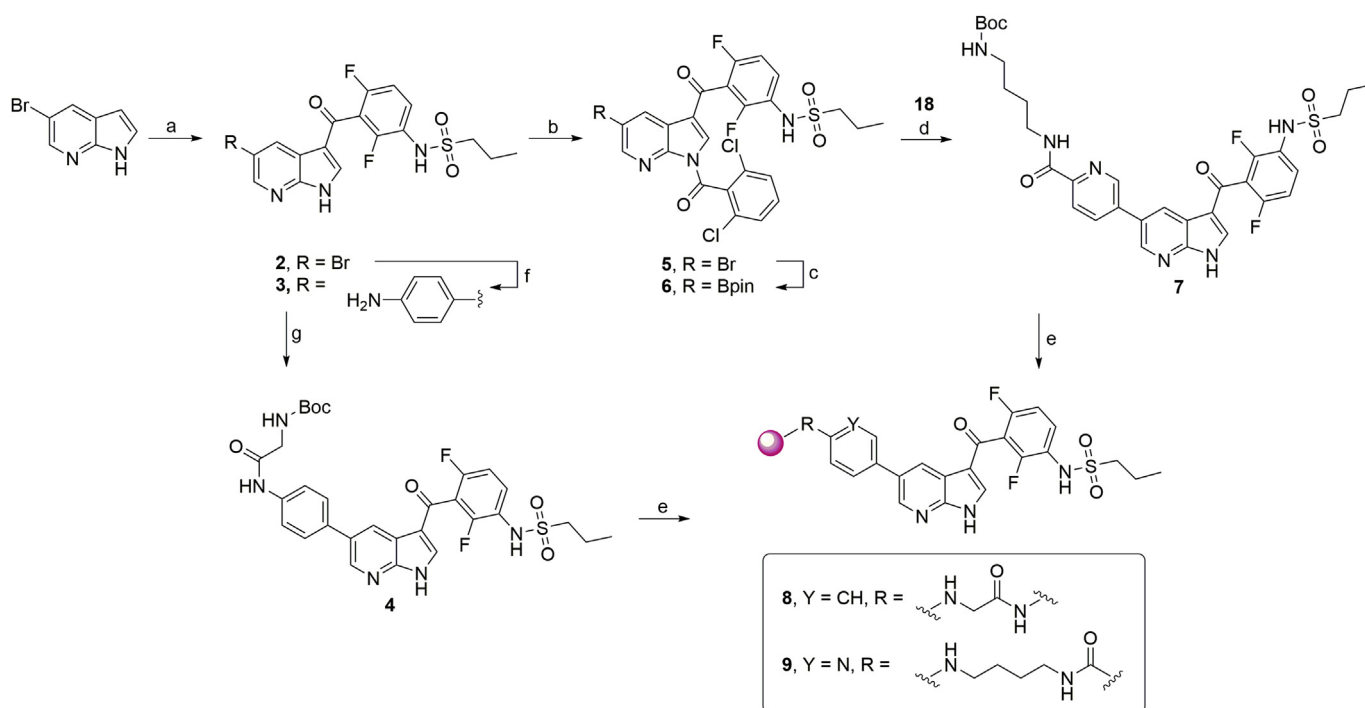


Fig. 3. Structures of azaindole (A) and α -carboline (B) scaffolds used as hinge-binding motives.

**Scheme 1.** Synthesis of linkage systems 12–22.

^aReaction conditions: (a) HATU or HBTU or CDI, Et₃N or DIPEA, DMF or THF, RT, 17 h, 36–59%; (b) (i) (COCl)₂, DCM, DMF, RT, 1 h; (ii) corresponding amine, DMF, 0 °C, 3 h, 43% – quant.

**Scheme 2.** Synthesis of compound 8 and 9 with 5-TAMRA attached to derivatives with azaindole scaffold A.

^aReaction conditions: (a) AlCl₃, 2,6-difluoro-3-(propylsulfonamido)benzoic acid, (COCl)₂, DCM, 50 °C, 85%; (b) 2,6-dichlorobenzoyl chloride, Et₃N, DMAP, THF, 0 °C, 17 h, 68%; (c) B₂pin₂, KOAc, Pd(PPh₃)₂Cl₂, 1,4-dioxane, 80 °C, 2 h, 68%; (d) K₂CO₃, Pd(PPh₃)₄, 1,4-dioxane/H₂O (1:1, v/v), 55 °C, 72 h, 49%; (e) 5-TAMRA, HATU, DIPEA, DMF, rt, 17 h, 30–73%; (f) 4-(4,4,5,5-tetramethyl-1,3,2-dioxaborolan-2-yl)aniline, K₂CO₃, Pd(PPh₃)₄, MW (50 W) 1,4-dioxane/H₂O (1:1, v/v), 110 °C, 40 min, 52%; (g) *tert*-butoxycarbonyl glycine, DIPEA, HATU, DMF, rt, 17 h, 84%.

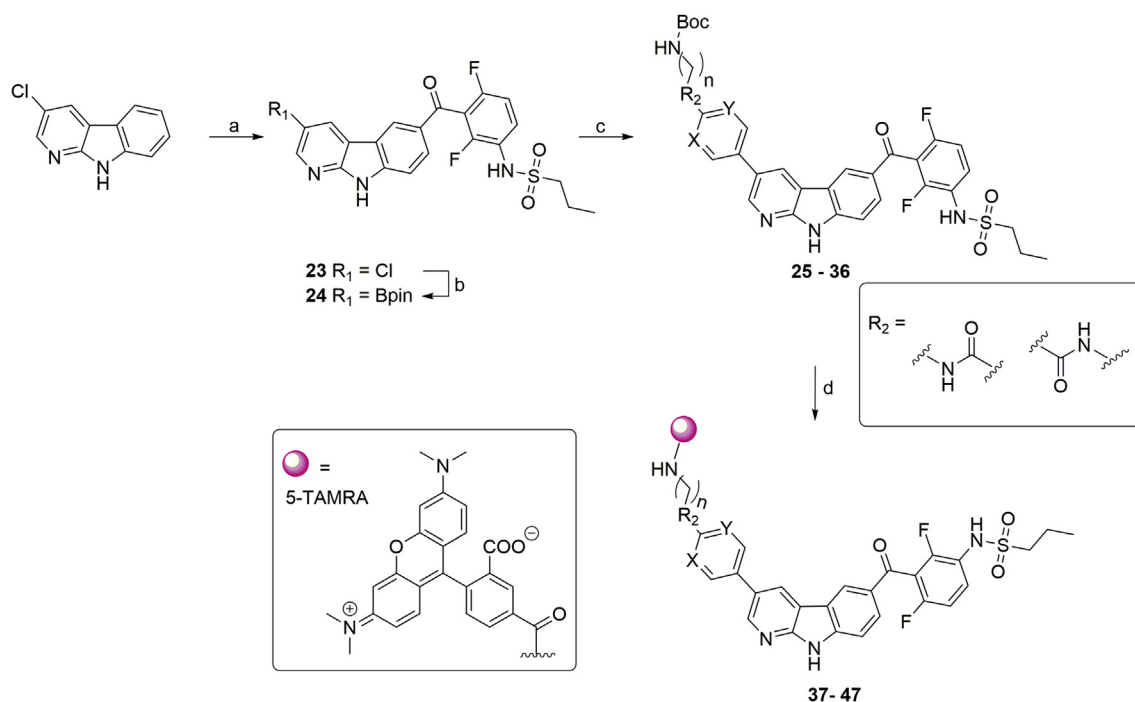
Surprisingly, the selectivity profile (Fig. 5) of compound **45** reveals no binding to the off-target BRAF (POC^{BRAF} = 92) which is the target for **1** that was used as a starting point for the ligand design. The superimposition of the docking pose of **45** bound to MKK4 and the crystal structure of BRAF in complex with **1** demonstrates that BRAF is missing the cleft outside the binding pocket, which allows the beneficial positioning of the 5-TAMRA moiety. The weak interaction between **45** and BRAF can be explained by severe steric clashes, especially related to BRAF residues D479, K473, W531 and E533.

Further investigations at lower assay concentrations on MKK4 (Table 3) showed that **45** reveals sustained high binding affinity.

To investigate whether compound **45** can be used to find new small molecules in a fluorescence polarization assay, we validated

the interaction of known inhibitors **53–55** of MKK4 (see SI) in the presence of **45** (Fig. 6) [14]. These compounds differ in their binding affinity towards MKK4. The positive control **53** has a high binding affinity to MKK4 with a POC of 0.25 at a concentration of 100 nM and showed an EC₅₀-value of 31 nM. The reference compound **54** has a weaker binding affinity to MKK4 (POC^{MKK4} = 11) than **53** and shows a decreased EC₅₀-value of 164 nM. **55** was used as negative control (POC^{MKK4} = 47) and resulted in an EC₅₀-value of 628 nM. Using MKK4 at 64 nM and compound **45** at 20 nM in a competition binding experiment, all known inhibitors showed EC₅₀-values fitting their binding properties and could be properly classified.

Hence, compound **45** is a promising candidate which can be implemented for fluorescence polarization high-throughput-



Scheme 3. Synthesis of compound **37–47** with 5-TAMRA attached to derivatives with α -carboline scaffold **B**.

^aReaction conditions: (a) AlCl_3 , 2,6-difluoro-3-(propylsulfonamido)benzoic acid, $(\text{COCl})_2$, DCM, 50 °C, 17 h, 69%; (b) B_2pin_2 , KOAc, XPhos Pd G3, MW (50 W), 1,4-dioxane, 110 °C, 40 min, 89%; (c) appropriate linkages **12–22**, $\text{Pd}(\text{PPh}_3)_4$, K_2CO_3 , 1,4-dioxane/ H_2O (1:1, v/v), MW (50 W), 110 °C, 40 min, 24–65%; (d) (i) toluene/TFA (10:1, v/v), (ii) 5-TAMRA, HATU, DIPEA, DMF, rt, 17 h, 20–65%.

screening to find new small molecule MKK4 inhibitors from large compound libraries.

5. Conclusion

In this study we report on the design of a fluorescent compound addressing the molecular target MKK4 with high affinity. Installing the bulky fluorophore 5-TAMRA and an appropriate linker at the *para*-chloro side of **1** has no negative effect on binding and confirms the assumption about the orientation of **1** bound to MKK4 based on docking experiments. For targeting MKK4 with a fluorescent tool compound, the linker system of **45** comprising four carbons appears the most promising. Moreover, changing the propyl residue of **1** to more lipophilic residues increases the binding affinity. Also, the replacement of the azaindole- to an α -carboline-core is well-tolerated.

Compound **45** was designed based on the information of the off-target activity of **1** towards MKK4 and represents a potent fluorescent ligand which can be used for a high-throughput screen to find new chemical entities as promising MKK4 inhibitors. Additionally, the results obtained herein provide insight into the possible binding mode of **1** to MKK4.

6. Experimental

Molecular modelling: All the molecular modelling was conducted with Maestro (Schrödinger Release 2019-3: Maestro, Schrödinger, LLC, New York, NY, 2019) with OPLS3 and OPLS3e force fields [16,17].

For the docking we used the Desmond [18] MD simulation-derived structure of MKK4 (derived from PDB ID: 3alo) which was prepared with Protein Preparation Wizard using default settings [19]. Prior to the docking, the ligands were prepared with LigPrep (Schrödinger, LLC, New York, NY, 2019). Finally, the Induced

Fit docking [20–22] was conducted using default parameters with extra precision (XP) accuracy.

The figures were generated with PyMOL (The PyMOL Molecular Graphics System, Version 2.0 Schrödinger, LLC.).

Biological assays: All compounds were investigated by a commercial binding assay by DiscoverX (Kinomescan™) at a screening concentration of 100 nM, which uses an immobilised ligand competing with the measured compound for the kinase. For identification of compound **45** as a probe for HTS, a fluorescence polarization assay with MKK4 and known inhibitors of the kinase was established [23].

Materials: All reagents and (anhydrous) solvents are commercially available and were used without further purification.

NMR: ^1H and ^{13}C NMR spectra were obtained with Bruker Avance 200, Bruker Avance 400 or Bruker Avance 600. The spectra were obtained in the indicated solvent and calibrated against the residual proton peak of the deuterated solvent. Chemical shifts (δ) are reported in parts per million.

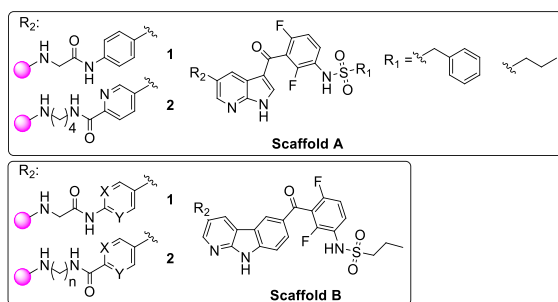
Mass Spectrometry: Mass spectra were obtained by TLC-MS (ESI) and from the Mass Spectrometry Department (HRMS), Institute of Organic Chemistry, Eberhard Karls Universität Tübingen.

TLC: Analyses were performed on fluorescent silica gel 60 F254 plates (Merck) and visualized under UV illumination at 254 and 366 nm.

Column Chromatography. Column chromatography was performed on DAVISIL LC60A 20–45 μm silica from Grace Davison and Geduran Si60 63–200 μm silica from Merck for the precolumn using an Interchim PuriFlash 430 automated flash chromatography system.

HPLC: The purity of all compounds is, unless otherwise stated, >95% and was determined via reverse-phase high-performance liquid chromatography on Hewlett-Packard HP 1090 series II LC equipped with a UV diode array detector (DAD, detection at 230 and 254 nm). The chromatographic separation was performed on a

Table 1
Binding affinities of the synthesized fluorescent derivatives on MKK4.



Compound	Scaffold ^a	R ₁	Linker		MKK4 ^b [POC]	
			n	R ₂ ^c X, Y		
8	A	Propyl	1	1	-	11.0
9	A	Propyl	4	2	-	57.0
10	A	Benzyl	1	2	-	6.6
11	A	Benzyl	4	2	-	13.0
37	B	Propyl	1	1	X, Y = CH	13.0
38	B	Propyl	2	2	X, Y = CH	19.0
39	B	Propyl	3	2	X, Y = CH	13.0
40	B	Propyl	4	2	X, Y = CH	4.3
41	B	Propyl	5	2	X, Y = CH	32.0
42	B	Propyl	6	2	X, Y = CH	6.6
43	B	Propyl	1	1	X = N Y = CH	8.4
44	B	Propyl	3	2	X = N Y = CH	4.5
45	B	Propyl	4	2	X = N Y = CH	1.3
46	B	Propyl	6	2	X = N Y = CH	4.8
47	B	Propyl	4	2	X, Y = N	9.3
1	A	Propyl	-	-	-	14.0

^a Scaffold: (A) azaindole, (B) α -carboline.

^b Screening concentration 100 nM.

^c R₂: 1 = Retroamide, 2 = Amide.

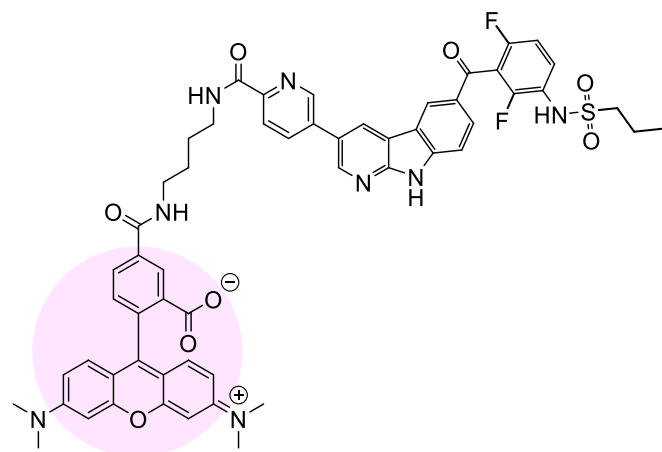


Fig. 4. Structure of compound **45** (fluorophore highlighted in pink). (For interpretation of the references to color in this figure legend, the reader is referred to the Web version of this article.)

Phenomenex Luna 5u C8 column (150 mm \times 4.6 mm, 5 μ m) at 35 $^{\circ}$ C oven temperature. The injection volume was 5 μ L, and the gradient of the used method was the following (flow, 1.5 mL/min), with 0.01 M KH₂PO₄, pH 2.3 (solvent A), methanol (solvent B): from 40% B to 85% B in 8 min, 85% B for 5 min, from 85% to 40% B in 1 min, 40% B for 2 min, stop time 16 min.

7. Synthesis

The representative preparation of compound **45** is given. All other compounds were synthesized following similar procedures. Detailed descriptions and analytics can be found in the Supporting Information.

7.1. *N*-(3-(3-chloro-9*H*-pyrido[2,3-*b*]indole-6-carbonyl)-2,4-difluorophenyl)propane-1-sulfonamide (**23**)

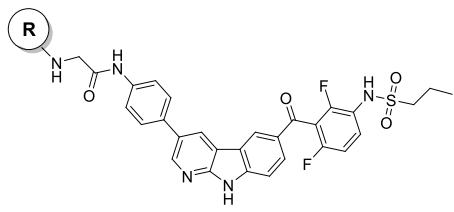
3-Chloro-9*H*-pyrido[2,3-*b*]indole (1.03 g, 5.08 mmol, 1 eq) and AlCl₃ (3.39 g, 25.41 mmol, 5 eq) were dissolved in DCM (50 mL), and stirred at room temperature for 60 min. Meanwhile, 2,6-difluoro-3-(propylsulfonamido)benzoic acid (2.13 g, 7.62 mmol, 1.5 eq) was suspended in DCM (20 mL) and oxalyl chloride (654 μ L, 1.5 mmol, 1.5 eq) and DMF (500 μ L) were added dropwise. After the gas evolution stopped, both mixtures were combined and stirred at 50 $^{\circ}$ C until no starting material was left. The reaction was stopped by adding MeOH and water at 0 $^{\circ}$ C, the aqueous phase was then extracted with ethyl acetate. The organic phase was concentrated and the forming precipitate (1.53 g, 3.3 mmol, 65%) was collected and dried under vacuum conditions. ¹H NMR (200 MHz, DMSO) δ 12.63 (s, 1H), 9.85 (s, 1H), 8.88 (d, *J* = 1.8 Hz, 1H), 8.80 (s, 1H), 8.48 (d, *J* = 2.0 Hz, 1H), 8.06 (d, *J* = 8.6 Hz, 1H), 7.75–7.60 (m, 2H), 7.34 (t, *J* = 8.7 Hz, 1H), 3.21–3.11 (m, 2H), 1.85–1.61 (m, 2H), 0.93 (t, *J* = 7.3 Hz, 3H) ppm. ¹³C NMR (50 MHz, DMSO) δ 187.1, 156.22 (dd, *J* = 246.8, 6.8 Hz), 152.38 (dd, *J* = 250.0, 8.4 Hz), 151., 145.4, 143.8, 129.4, 129.2, 128.6, 128.3, 128.47 (d, *J* = 7.5 Hz), 125.8, 123.1, 122.14 (dd, *J* = 13.4, 3.7 Hz), 119.9, 117.52 (dd, *J* = 23.9, 22.1 Hz), 116.8, 112.60 (dd, *J* = 21.5, 2.5 Hz), 112.4, 53.5, 16.9, 12.6 ppm. ESI-MS (^{m/z}) 462.1 [M-H]⁻.

7.2. *N*-(2,4-difluoro-3-(3-(4,4,5,5-tetramethyl-1,3,2-dioxaborolan-2-yl)-9*H*-pyrido[2,3-*b*]indole-6-carbonyl)phenyl)propane-1-sulfonamide (**24**)

N-(3-(3-chloro-9*H*-pyrido[2,3-*b*]indole-6-carbonyl)-2,4-difluorophenyl)propane-1-sulfonamide (514 mg, 1.1 mmol, 1 eq), 4,4,4',4',5,5',5'-octamethyl-2,2'-bi(1,3,2-dioxaborolane) (295 mg, 1.16 mmol, 1.1 eq) and KOAc (217 mg, 2.2 mmol, 2 eq) were suspended in 1,4-dioxane/H₂O (1:1, v/v, 4 mL) and purged with argon for 15 min. Subsequently XPhos Pd G3 (29 mg, 33 μ mol, 3 mol %) was added and stirred under microwave irradiation (50 W, 115 $^{\circ}$ C) for 40 min. After TLC analysis revealed full consumption of the starting material, ethyl acetate was added, and the organic layer was washed with water and saturated sodium chloride solution. The organic layer was dried over sodium sulfate and the solvent was removed under vacuum conditions. After column chromatography (DCM/EE, v/v, 0–50 %), the pure product could be obtained as an off-white solid (550 mg, 990 μ mol, 89 %). ¹H NMR (200 MHz, DMSO) δ 12.54 (s, 1H), 9.78 (s, 1H), 8.96 (s, 1H), 8.87 (s, 1H), 8.71 (s, 1H), 8.09 (d, *J* = 9.0 Hz, 1H), 7.72–7.57 (m, 1H), 7.33 (t, *J* = 8.7 Hz, 1H), 3.24–3.08 (m, 1H), 1.74 (dd, *J* = 15.1, 7.5 Hz, 1H), 1.33 (s, 3H), 0.93 (t, *J* = 7.3 Hz, 1H) ppm. ¹³C NMR (101 MHz, DMSO) δ 187.6, 158.0, 157.9, 157.9, 156.69 (dd, *J* = 246.7, 6.7 Hz), 155.5, 155.4, 155.4, 154.8, 154.1, 154.0, 153.4, 152.79 (dd, *J* = 249.2, 8.0 Hz), 151.6, 151.5, 143.4, 136.5, 129.65 (d, *J* = 9.3 Hz), 129.2, 127.8, 126.6, 122.40 (dd, *J* = 13.2, 3.2 Hz), 121.1, 118.00 (t, *J* = 22.9 Hz), 115.7, 112.92 (dd, *J* = 22.7, 3.8 Hz), 112.6, 84.3, 53.9, 25.1, 17.1, 13.0 ppm. ESI-MS (^{m/z}) 554.1 [M-H]⁻.

Table 2

Binding affinities of Boc-protected carboline **25** and the corresponding 5-TAMRA derivative **37**.



Compound	R	MKK4 ^b [POC]
25	Boc	9.2
37	5-TAMRA	13.0

^b Screening concentration 100 nM.

Compound	BRAF	MKK4
	[POC] at 100 nm	
45	92	1

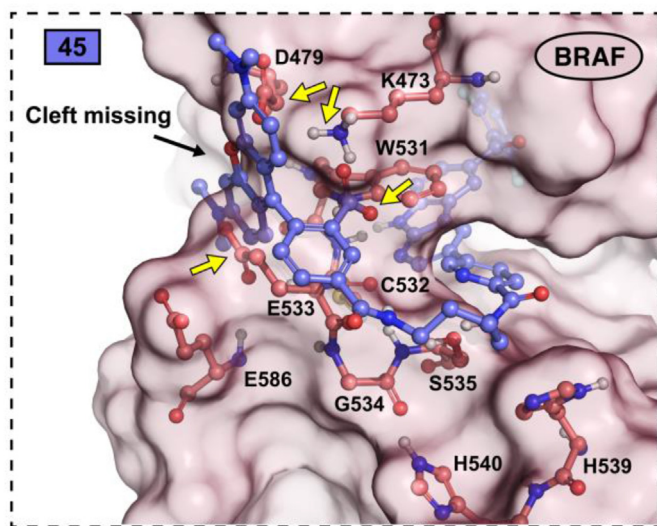


Fig. 5. Compound **45** is selective for MKK4 with low affinity towards BRAF. Superimposition of docking pose of **45** (purple) in MKK4 (hidden) and the crystal structure of BRAF (PDB ID: 4rzv) (see Fig. 2A and C). The nearby amino acids of BRAF within 4 Å of **45** are highlighted in red in the figures. The yellow arrows indicate the major sterically clashes between BRAF and **45**. The molecular surface of BRAF is shown in red surface. (For interpretation of the references to color in this figure legend, the reader is referred to the Web version of this article.)

7.3. *Tert*-butyl (4-(4-(6-(2,6-difluoro-3-(propylsulfonamido)benzoyl)-9H-pyrido[2,3-b]indol-3-yl)benzamido)butyl)carbamate (**34**)

N-(2,4-difluoro-3-(3-(4,4,5,5-tetramethyl-1,3,2-dioxaborolan-2-yl)-9H-pyrido[2,3-b]indole-6-carbonyl)phenyl)propane-1-sulfonamide (200 mg, 360 μmol, 1 eq), *tert*-butyl (4-(4-bromobenzamido)butyl)carbamate (147 mg, 396 μmol, 1.1 eq) and K₂CO₃ (100 mg, 720 μmol, 2 eq) were suspended in 1,4-dioxane/H₂O (1:1, v/v, 3.5 mL) and purged with argon for 15 min. Subsequently Pd(PPh₃)₄ (21 mg, 18 μmol, 5 mol %) was added and stirred

Table 3

Binding affinities of **45** at different screening concentrations.

Compound	MKK4 [POC]		
	100 nM	30 nM	10 nM
45	1.3	4.1	18.0

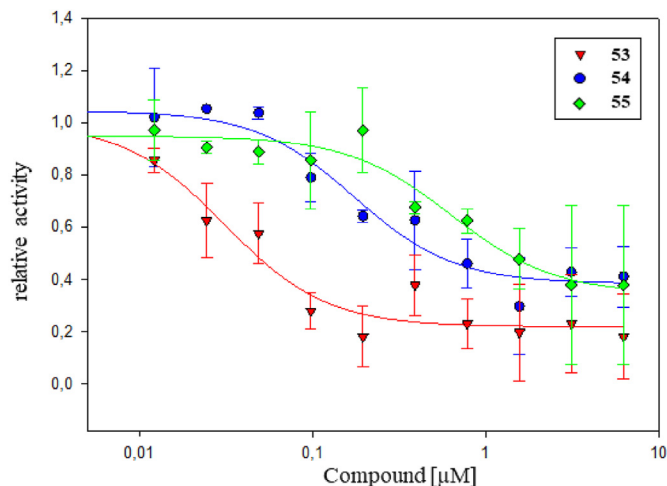


Fig. 6. MKK4 Fluorescence polarization assay. Compound **45** in competition with MKK4 inhibitors **53** (red), **54** (blue) and **55** (green) showed EC₅₀-values of 31, 164 and 628 nM respectively. (For interpretation of the references to color in this figure legend, the reader is referred to the Web version of this article.)

under microwave irradiation (50 W, 110 °C) for 45 min. After TLC analysis revealed full consumption of the starting material, ethyl acetate was added, and the organic layer was washed with water and saturated sodium chloride solution. The organic layer was dried over sodium sulfate and the solvent was removed under vacuum conditions. After column chromatography (DCM/EE, v/v, 0–75 %) the pure product could be obtained as a colorless solid (199 mg, 271 μmol, 75 %). ¹H NMR (200 MHz, DMSO) δ 12.57 (s, 1H), 9.83 (s, 1H), 9.14 (d, *J* = 2.1 Hz, 1H), 8.90 (d, *J* = 2.0 Hz, 1H), 8.85 (s, 1H), 8.53 (t, *J* = 5.6 Hz, 1H), 8.10–7.87 (m, 5H), 7.76–7.58 (m, 2H), 7.35 (t, *J* = 8.7 Hz, 1H), 6.81 (t, *J* = 5.4 Hz, 1H), 3.28 (d, *J* = 5.6 Hz, 2H), 3.22–3.11 (m, 2H), 2.95 (d, *J* = 6.0 Hz, H), 1.85–1.62 (m, 2H), 1.47 (s, 4H), 1.37 (s, 9H), 0.92 (t, *J* = 7.4 Hz, 3H) ppm. ¹³C NMR (50 MHz, DMSO) δ 187.0, 165.7, 155.6, 152.5, 146.1, 143.5, 140.5, 133.2, 128.4, 127.9, 127.8, 126.5, 120.8, 115.7, 77.4, 53.5, 39.5, 28.3, 16.8, 12.6 ppm. ESI-MS (^{m/z}) 742.8 [M+Na]⁺.

7.4. 5-((4-(5-(6-(2,6-Difluoro-3-(propylsulfonamido)benzoyl)-9H-pyrido[2,3-b]indol-3-yl)picolinamido)butyl)carbamoyl)-2-(6-(dimethylamino)-3-(dimethyliminio)-3H-xanthen-9-yl)benzoate (**45**)

Tert-butyl (4-(5-(6-(2,6-difluoro-3-(propylsulfonamido)benzoyl)-9H-pyrido[2,3-b]indol-3-yl)picolinamido)butyl)carbamate (109 mg, 134 μmol, 2.5 eq) was dissolved in toluene/TFA (10:1, v/v) and stirred for 17 h. Then the solvent was evaporated under reduced pressure and the residue was dissolved again in DMF (0.5 mL). The mixture was added to a solution of 5-TAMRA (23 mg, 53 μmol, 1 eq), HATU (20 mg, 53 μmol, 1 eq) and DIPEA (75 μL, 427 μmol, 8 eq) in DMF (1 mL). After 17 h at room temperature the solvent was removed under reduced pressure. The crude product was purified using column chromatography (DCM/MeOH/TFA, v/v/v, 90:9.5:0.5) to obtain the pure product as a purple solid (27 mg, 25 μmol, 47 %). mp 195 - 197 °C, ¹H NMR (400 MHz, DMSO) δ 12.60

(s, 1H), 9.21 (d, $J = 2.2$ Hz, 1H), 9.10 (d, $J = 2.2$ Hz, 1H), 8.97 (t, $J = 2.4$ Hz, 1H), 8.87 (dd, $J = 11.2, 5.0$ Hz, 1H), 8.84 (s, 1H), 8.45 (s, 1H), 8.41 (dd, $J = 8.2, 2.2$ Hz, 1H), 8.23 (dd, $J = 8.1, 1.5$ Hz, 1H), 8.16 (d, $J = 8.2$ Hz, 1H), 8.03 (dd, $J = 8.6, 1.6$ Hz, 1H), 7.69 (d, $J = 8.8$ Hz, 1H), 7.64 (dt, $J = 9.1, 4.6$ Hz, 1H), 7.32 (t, $J = 7.9$ Hz, 1H), 6.54–6.45 (m, 6H), 3.42–3.35 (m, 4H), 3.17–3.08 (m, 2H), 2.93 (s, 12H), 1.72 (td, $J = 15.0, 7.5$ Hz, 2H), 1.63 (s, 4H), 0.91 (t, $J = 7.4$ Hz, 3H) ppm. HPLC $t_R = 6.633$ min, purity: 96 % (254.4 nm), 100 % (430.4 nm). IR (ATP) [cm^{-1}] 1597, 1490, 1347, 1184, 1139. ESI-HRMS m/z $[\text{M}+\text{H}]^+$ calculated: 1033.35131, measured: 1033.35050.

Author contributions

All authors contributed to writing the manuscript. All authors have approved the final version of the manuscript.

Notes

The authors declare no competing financial interest.

Declaration of competing interest

The authors declare the following financial interests/personal relationships which may be considered as potential competing interests: SL is stock owner <3% of Heparegenix GmbH. However this relationship has not influenced any work related to this manuscript.

Acknowledgements

We would like to thank the CSC – IT Center for Science, Finland for computational resources. T.P. acknowledges European Union's Horizon 2020 research and innovation programme (Marie Skłodowska-Curie grant agreement No 839230) and the Orion Research Foundation sr for financial support.

We would like to thank Kristine Schmidt for the language proofreading.

Appendix A. Supplementary data

Supplementary data related to this article can be found at <https://doi.org/10.1016/j.ejmech.2020.112901>.

References

- [1] T. Wuestefeld, M. Pesic, R. Rudalska, D. Dauch, T. Longerich, T.-W. Kang, T. Yeves, F. Heinzmann, L. Hoenicke, A. Hohmeyer, A. Potapova, I. Rittelmeyer, M. Jarek, R. Geffers, M. Scharfe, F. Klawonn, P. Schirmacher, N.P. Malek, M. Ott, A. Nordheim, A. Vogel, M.P. Manns, L. Zender, A Direct in vivo RNAi screen identifies MKK4 as a key regulator of liver regeneration, *Cell* 153 (2013) 389–401.
- [2] W. Haeusgen, T. Herdegen, V. Waetzig, The bottleneck of JNK signaling: molecular and functional characteristics of MKK4 and MKK7, *Eur. J. Cell Biol.* 90 (2011) 536–544.
- [3] H. Vin, S.S. Ojeda, G. Ching, M.L. Leung, V. Chitsazzadeh, D.W. Dwyer, C.H. Adelmann, M. Restrepo, K.N. Richards, L.R. Stewart, L. Du, S.B. Ferguson, D. Chakravarti, K. Ehrenreiter, M. Baccarini, R. Ruggieri, J.L. Curry, K.B. Kim, A.M. Ciurea, M. Duvic, V.G. Prieto, S.E. Ullrich, K.N. Dalby, E.R. Flores, K.Y. Tsai, BRAF inhibitors suppress apoptosis through off-target inhibition of JNK signaling, *Elife* 2 (2013) 1–25.
- [4] F. Ansideri, A. Lange, A. El-Gokha, F.M. Boeckler, P. Koch, Fluorescence polarization-based assays for detecting compounds binding to inactive c-Jun N-terminal kinase 3 and p38 α mitogen-activated protein kinase, *Anal. Biochem.* 503 (2016) 28–40.
- [5] J. Inglese, C.E. Shamu, R.K. Guy, Reporting data from high-throughput screening of small-molecule libraries, *Nat. Chem. Biol.* 3 (2007) 438–441.
- [6] M.D. Hall, A. Yasgar, T. Peryea, J.C. Braisted, A. Jadhav, A. Simeonov, N.P. Coussens, Fluorescence polarization assays in high-throughput screening and drug discovery: a review, *Methods Appl. Fluoresc.* 4 (2016) 22001.
- [7] H. Mikula, S. Stapleton, R.H. Kohler, C. Vinegoni, R. Weissleder, Design and development of fluorescent vemurafenib analogs for in vivo imaging, *Theranostics* 7 (2017) 1257–1265.
- [8] Z. Karoulia, E. Gavathiotis, P.I. Poulikakos, New perspectives for targeting RAF kinase in human cancer, *Nat. Rev. Canc.* 17 (2017) 676–691.
- [9] G. Bollag, P. Hirth, J. Tsai, J. Zhang, P.N. Ibrahim, H. Cho, W. Spevak, C. Zhang, Y. Zhang, G. Habets, E.A. Burton, B. Wong, G. Tsang, B.L. West, B. Powell, R. Shellooe, A. Marimuthu, H. Nguyen, K.Y.J. Zhang, D.R. Artis, J. Schlessinger, F. Su, B. Higgins, R. Iyer, K. D'Andrea, A. Koehler, M. Stumm, P.S. Lin, R.J. Lee, J. Grippo, I. Puzanov, K.B. Kim, A. Ribas, G.A. McArthur, J.A. Sosman, P.B. Chapman, K.T. Flaherty, X. Xu, K.L. Nathanson, K. Nolop, Clinical efficacy of a RAF inhibitor needs broad target blockade in BRAF-mutant melanoma, *Nature* 467 (2010) 596–599.
- [10] Takashi Matsumoto, Takayoshi Kinoshita, Yasuyuki Kirii, Toshiji Tada, Akihito Yamano, Crystal and solution structures disclose a putative transient state of mitogen-activated protein kinase kinase 4, *Biochem. Biophys. Res. Commun.* 425 (2012) 195–200.
- [11] T. Matsumoto, T. Kinoshita, Y. Kirii, K. Yokota, K. Hamada, T. Tada, Crystal structures of MKK4 kinase domain reveal that substrate peptide binds to an allosteric site and induces an auto-inhibition state, *Biochem. Biophys. Res. Commun.* 400 (2010) 369–373.
- [12] E. Shevchenko, A. Poso, T. Pantsar, The autoinhibited state of MKK4: phosphorylation, putative dimerization and R134W mutant studied by molecular dynamics simulations, *Comput. Struct. Biotechnol. J.* 18 (2020) 2687–2698, <https://doi.org/10.1016/j.csbj.2020.09.017>.
- [13] T. Lowinger, M. Shimazaki, H. Sato, K. Tanaka, K. Marx, M. Yamamoto, K. Urbahns, F. Gantner, Hiromi Okigami, Kasake Nakashima, Keisuke Takeshita, K. Bacon, H. Komura, N. Yoshida, WO 03/037898 A1, 2003.
- [14] W. Albrecht, S. Laufer, R. Selig, P. Klöveborn, B. Praefcke WO 2018/134254 A1, 2018.
- [15] M. Juchum, R. Selig, S. Laufer, W. Albrecht, WO2019243315 A1, 2019.
- [16] E. Harder, W. Damm, J. Maple, C. Wu, M. Reboul, J.Y. Xiang, L. Wang, D. Lupyran, M.K. Dahlgren, J.L. Knight, J.W. Kaus, D.S. Cerutti, G. Krilov, W.L. Jorgensen, R. Abel, R.A. Friesner, OPLS3: a force field providing broad coverage of drug-like small molecules and proteins, *J. Chem. Theor. Comput.* 12 (2016) 281–296.
- [17] K. Roos, C. Wu, W. Damm, M. Reboul, J.M. Stevenson, C. Lu, M.K. Dahlgren, S. Mondal, W. Chen, L. Wang, R. Abel, R.A. Friesner, E.D. Harder, OPLS3e: extending Force Field Coverage for Drug-Like Small Molecules, *J. Chem. Theor. Comput.* 15 (2019) 1863–1874.
- [18] K.J. Bowers, D.E. Chow, H. Xu, R.O. Dror, M.P. Eastwood, B.A. Gregersen, J.L. Klepeis, I. Kolossvary, M.A. Moraes, F.D. Sacerdoti, J.K. Salmon, Y. Shan, D.E. Shaw, Scalable algorithms for molecular dynamics simulations on commodity clusters, in: *Scalable Algorithms for Molecular Dynamics Simulations on Commodity Clusters*, IEEE, Tampa, FL, 2006, p. 43.
- [19] G.M. Sastry, M. Adzhigirey, T. Day, R. Annabhimoju, W. Sherman, Protein and ligand preparation: parameters, protocols, and influence on virtual screening enrichments, *J. Comput. Aided Mol. Des.* 27 (2013) 221–234.
- [20] R. Farid, T. Day, R.A. Friesner, R.A. Pearlstein, New insights about HERG blockade obtained from protein modeling, potential energy mapping, and docking studies, *Bioorg. Med. Chem.* 14 (2006) 3160–3173.
- [21] W. Sherman, H.S. Beard, R. Farid, Use of an induced fit receptor structure in virtual screening, *Chem. Biol. Drug Des.* 67 (2006) 83–84.
- [22] W. Sherman, T. Day, M.P. Jacobson, R.A. Friesner, R. Farid, Novel procedure for modeling ligand/receptor induced fit effects, *J. Med. Chem.* 49 (2006) 534–553.
- [23] M.A. Fabian, W.H. Biggs, D.K. Treiber, C.E. Atteridge, M.D. Azimioara, M.G. Benedetti, T.A. Carter, P. Ciceri, P.T. Edeen, M. Floyd, J.M. Ford, M. Galvin, J.L. Gerlach, R.M. Grotzfeld, S. Herrgard, D.E. Insko, M.A. Insko, A.G. Lai, J.-M. Lélis, S.A. Mehta, Z.V. Milanov, A.M. Velasco, L.M. Wodicka, H.K. Patel, P.P. Zarrinkar, D.J. Lockhart, A small molecule-kinase interaction map for clinical kinase inhibitors, *Nat. Biotechnol.* 23 (2005) 329–336.